PERGAMON

International Journal of Heat and Mass Transfer 43 (2000) 3287–3298

International Journal of HEAT and MASS TRANSFER

www.elsevier.com/locate/ijhmt

Thermally controlled bubble collapse in binary solutions

T.L. Merrill*

McGowan Center for Artificial Organ Development, University of Pittsburgh, 300 Technology, Rm 307, Pittsburgh, PA 15219, USA

Received 20 October 1998; received in revised form 3 December 1999

Abstract

This paper theoretically analyzes thermally controlled bubble collapse in binary solutions. Using a finite difference approach with an adaptive grid, three aspects of bubble collapse are investigated: counter-diffusion, initial bubble diameter, and absorber cooling rate. Results illustrate how counter-diffusion of the absorbent, acting to preserve the bubble life span, is offset by convective mass transfer arising from bubble interface motion. Predicted bubble mass transfer rates for an ammonia water system increase with the square of the bubble radius (diameters: 1.8–5.6 mm) and with increased absorber cooling rates. Model predictions compare well with simple semi-empirical correlations for bubble heat and mass transfer coefficients.

1. Introduction

Today's absorption chiller manufacturers continue to use physically large shell and tube absorbers conceived decades ago. To improve absorption chiller competitiveness relative to its sibling technology, the vapor compression chiller, new methods for absorber size and cost reduction are being researched. One such method is bubble absorption. Bubble absorbers provide an effective way to place absorbent vapor into direct and intimate contact with the absorbate liquid. This paper presents a theoretical analysis of a single bubble absorbed into a subcooled binary liquid solution. While the equations presented are general in nature, the components used for this study are ammonia and water — a typical binary mixture used in absorption cycles.

There has been extensive work on bubble dynamics. Bubble fluid dynamics research conducted over 30 years back by Levich [1], Chao [2], and Moore [3] correctly predicted the liquid velocity field surrounding a rising bubble. Pure heat transfer studies with no mass transfer and pure mass transfer studies with no heat transfer are also plentiful. In particular, Azbel [4] and Florsheutz and Chao [5] provide detailed theoretical and experimental information regarding single-mode transfer cases (pure heat or mass transfer).

However, there is comparatively little information available on coupled heat and mass transfer involving dispersed bubbles in liquids. Elperin and Fominykh [6] have recently presented a cell model for multiple stationary bubbles in non-isothermal absorption. In falling films, coupled heat and mass transfer has been studied by numerous researchers [7–11]. Ruh and Smith [12] have theoretically studied the effect of counter-diffusion on gas-side mass transfer resistance in a stirred tank reactor.

The objective of this paper is to provide a detailed description of a binary bubble undergoing absorption within a subcooled binary liquid. It will address the following questions:

1. Looking at average transport variables such as the average bubble heat and mass transfer coefficients,

* Tel.: +1-412-383-9498; fax: +1-412-383-9460.
E-mail address: merrilltl@msx.upmc.edu (T.L. Merrill).

0017-9310/00/$ - see front matter
PII: S0017-9310(99)00383-X

Nomenclature

a	bubble radius (m)
c_p	specific heat (J/kg/K)
D_{ij}	general binary diffusivity coefficient (m^2/s)
d_e	bubble diameter (m)
D_{AB}	binary diffusivity coefficient of ammonia in water (m^2/s)
D_{BA}	binary diffusivity coefficient of water in ammonia (m^2/s)
h_{abs}	heat of vaporization and dilution (J/kg)
h_{fg}	heat of vaporization
$\bar{h}_m$	mass transfer coefficient (m/s)
$\bar{h}$	heat transfer coefficient ($W/m^2/K$)
$h_{f,I}$	liquid enthalpy of a component evaluated at the interface temperature (J/kg)
h_v	vapor enthalpy (J/kg)
h_l	liquid enthalpy (J/kg)
i	tangential position
j	radial position
k	thermal conductivity (W/m/K)
m_{bub}	bubble mass (kg)
$\overline{Nu}$	bubble Nusselt number, $\bar{h}d_e/k$
P	pressure (kPa)
Pe	heat transfer Péclet number, $U_t d_e/\kappa$
Pe_m	mass transfer Péclet number, $U_t d_e/D_{ij}$
Pe_{mesh}	heat transfer mesh Péclet number, $u_r \Delta r/\kappa$
$Pe_{mesh,m}$	mass transfer mesh Péclet number, $u_r \Delta r/D_{ij}$
Pr	Prandtl number, ν/κ
Re	Reynolds Number, $U_t d_e/\nu$
r	radial coordinate (m)
$\overline{Sc}$	Schmidt Number, ν/D_{ij}
$\overline{Sh}$	average Sherwood number, $\bar{h}_m d_e/D_{ij}$
T	temperature (°C or K)
t	time (s)
u	velocity (m/s)
U_t	bubble terminal velocity (m/s)
v	velocity component normal to an interface (m/s)
z	coordinate in the direction of the bubble ascent (m)

Greek symbols

Γ	a general nondimensional term, i.e. the Peclet number
κ	thermal diffusivity (m^2/s)
ν	kinematic viscosity (m^2/s)
θ	spherical-polar angle, measured from the forward stagnation point (degrees)
ρ	mass concentration (kg/m^3)
ϕ	nondimensional general scalar variable or velocity potential function (m^2/s)
ψ	stream function (m^3/s)
ω	mass fraction
$\forall$	for all

Superscripts

$*$	nondimensional or local transfer coefficient
$\cdot$	time derivative
–	average

Subscripts

A	ammonia
B	water
f	liquid
ff	far-field
g	gas or vapor
i	initial or theta location
itf	interface
j	radial location
l	liquid
n	normal direction
p	constant pressure
r	radial direction or relative
t	terminal
v	vapor
θ	theta direction or dependent on the theta location

how does the proposed model compare with existing semi-empirical correlations?

2. How does each component within a binary bubble behave as a bubble undergoes absorption into a binary liquid solution? In particular, how does the bubble react to the counter-diffusion of the absorbate?
3. How does initial bubble size and liquid flow field temperature gradient influence bubble collapse?

Following the problem formulation, including simplifying assumptions, the mathematical problem is forged. Having arranged the governing coupled partial differential equations with their required boundary and initial conditions, the numerical solution approach is briefly outlined. A benchmark model solution for heat and mass transfer about a collapsing bubble is then presented. Additional model solutions form a parametric study of the effects of the initial bubble diameter and the absorber cooling rate on bubble collapse. A direct comparison of model predictions with single bubble experimental data is not presented.

2. Analysis

Fig. 1 illustrates the initial multi-phase flow regime within a bubble absorber. Bubbles are injected into a binary liquid mixture through a multi-port injector. As the bubbles rise, the solution around it is subcooled by counter-current flowing coolant. The heat removed is the heat of absorption, which includes the heat of condensation and dilution. The absorption of numerous bubbles gradually raises the ammonia concentration in the liquid solution. Without the coolant, mass transfer would cease, the liquid concentration change would be inadequate, and the absorption cycle would stop.

Fig. 2 shows the model control volume and the fixed coordinate system at the bubble center of mass — a Lagrangian approach. True bubble absorption is complex, involving interacting bubbles swarms inside a turbulent liquid flow field. To make a solution tractable, several key assumptions were needed. These assumptions are shown in Table 1, organized in terms of the dispersed media, vapor, the continuous media, liquid, and the vapor–liquid interface [13,14].

2.1. Liquid flow field surrounding the bubble

The no-slip boundary condition can be relaxed at the bubble vapor–liquid interface, and in 1966, Wittke [15] described the flow field about a bubble that is translating and either collapsing or growing in size. The radial and tangential components of the liquid surrounding the bubble may be described as

$$u_r = -\frac{\partial \phi}{\partial r} = \frac{1}{r^2 \sin\theta}\frac{\partial \psi}{\partial \theta} - U_t\left(1 - \frac{a^3}{r^3}\right)\cos\theta + \frac{a^2 \dot{a}}{r^2} \quad (1)$$

and

$$u_\theta = -\frac{1}{r}\frac{\partial \phi}{\partial \theta} = -\frac{1}{r\sin\theta}\frac{\partial \psi}{\partial r} = U_t\left(1 + \frac{a_3}{2r^3}\right)\sin\theta, \quad (2)$$

where U_t is the terminal velocity of the bubble at various stages during bubble ascent. From a Lagrangian frame of reference, U_t can also be considered the approach velocity of the subcooled binary liquid. The term $\dot{a}$ represents the rate at which the bubble interface changes with time.

2.2. Governing conservation equations and boundary conditions

After making the boundary layer assumption that the gradient of mass fraction in the radial direction is significantly larger than that in the tangential direction, the mass fraction of ammonia (ω) in the subcooled liquid surrounding the bubble responds to the following non-dimensional conservation equation:

$$\frac{\partial \omega}{\partial t} + u_r\frac{\partial \omega}{\partial r} + \frac{u_\theta}{r}\frac{\partial \omega}{\partial \theta} = \frac{2}{ReSc}\left[\frac{1}{r^2}\frac{\partial}{\partial r}\left(r^2\frac{\partial \omega}{\partial r}\right)\right], \quad (3)$$

where the asterisks indicating a non-dimensional variable have been dropped.

Non-dimensional terms in Eq. (3) are defined in the following manner:

$$\omega^* = \frac{\omega(r,\theta,t)}{\omega_i}, \quad u_r^* = \frac{u_r}{U_t(t)}, \quad u_\theta^* = \frac{u_\theta}{U_t(t)}, \quad r^* = \frac{r}{a(t)}, \quad \text{and} \quad t^* = \frac{U_t(t)t}{a(t)}. \quad (4)$$

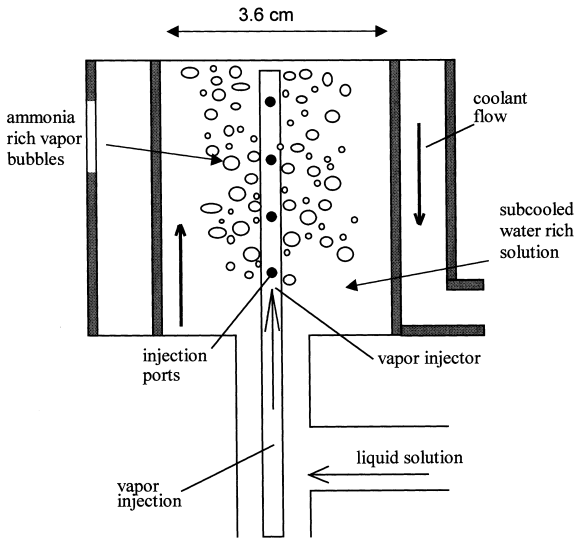

Fig. 1. Typical bubble absorption multi-phase flow field at an injection site.

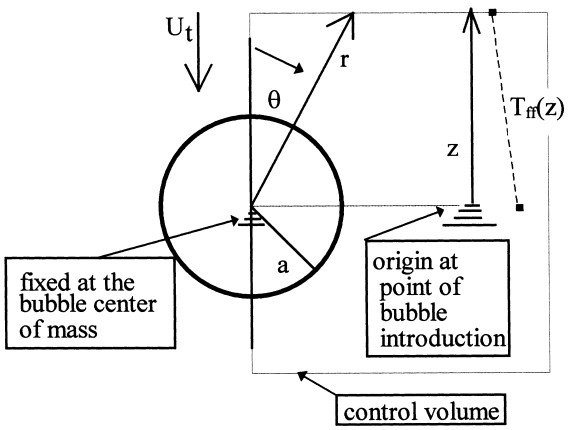

Fig. 2. Model control volume and fixed coordinate system at the bubble center of mass.

With the identical boundary layer assumption, the conservation of energy equation for the subcooled liquid surrounding a collapsing bubble takes on a similar form (asterisks have been dropped):

$$\frac{\partial T}{\partial t} + u_r \frac{\partial T}{\partial r} + \frac{u_\theta}{r}\frac{\partial T}{\partial \theta} = \frac{2}{Pe}\left[\frac{1}{r^2}\frac{\partial}{\partial r}\left(r^2\frac{\partial T}{\partial r}\right)\right], \tag{5}$$

where the non-dimensional temperature is

$$T^* = \frac{T(r,\theta,t)}{T_i}. \tag{6}$$

To solve these equations under the assumptions made in Table 1, two sets of boundary conditions were established. The first set of boundary conditions address initial values, far-field values, and axisymmetric values; the second set address the bubble interface: conservation of mass, conservation of energy, and equilibrium.

In the first set of boundary conditions, at time equal to 0 in the liquid surrounding the bubble, the following initial conditions were adopted

$$\text{at } t = 0, \quad T = T_i \quad \text{and} \quad \omega = \omega_i \quad \forall\,\theta \text{ and } r \tag{7}$$

At time greater than zero, far from the bubble interface, the liquid temperature field surrounding the bubble continually changes but the liquid concentration field surrounding the single bubble remains relatively unchanged:

$$\text{for } t > 0, \text{ as } r \to \infty, \quad T = T_{ff}(z), \quad \forall\,\theta \tag{8}$$

and

$$\text{for } t > 0, \text{ as } r \to \infty, \quad \frac{\partial \omega}{\partial r} \to 0, \quad \forall\,\theta. \tag{9}$$

The far-field temperature profile, $T_{ff}(z)$, is based on experimental data, where thermocouples were located along the length of 0.8 m long bubble absorber [16].

With the assumption of axisymmetric flow, the following boundary condition is established

$$\text{for } t > 0, \text{ for } r \geq a, \quad \theta = 0 \text{ or } \pi, \quad \frac{\partial T}{\partial \theta} = \frac{\partial \omega}{\partial \theta} = 0. \tag{10}$$

In the second set of boundary conditions, conservation of mass at the bubble interface leads to a redefinition of the liquid radial velocity at the interface

$$u_r = \dot{a}\left(1 - \frac{\rho_v}{\rho_l}\right), \tag{11}$$

that leads to a change in the radial velocity defined in Eq. (1)

$$u_r = -\frac{\partial \phi}{\partial r} = -U_t\left(1 - \frac{a^3}{r^3}\right)\cos\theta + \frac{a^2}{r^2}\left[\dot{a}\left(1 - \frac{\rho_v}{\rho_l}\right)\right]. \tag{12}$$

Examining the energy balance boundary condition at the bubble interface, requires an understanding of the mass balances for each component at the interface:

$$\rho_{A,\,v}\left(v_{v,\,n} - \dot{a}\right) = -\rho D_{AB}\left.\frac{\partial \omega_A}{\partial r}\right|_{itf} + \rho_A\left(v_{l,\,n} - \dot{a}\right), \tag{13}$$

and

$$\rho_{B,\,v}\left(v_{v,\,n} - \dot{a}\right) = -\rho D_{BA}\left.\frac{\partial \omega_B}{\partial r}\right|_{itf} + \rho_B\left(v_{l,\,n} - \dot{a}\right), \tag{14}$$

where the vapor mass flux is balanced by the liquid mass flux. In single component bubble collapse, such as the condensation of a water vapor bubble, the energy balance at the bubble interface can be written simply as

Table 1
Bubble collapse model assumptions

Category	Description
Vapor	Shape: throughout collapse, the bubble shape is spherical and without surface oscillations. The Weber number is equal to 3.4. Flow: inside the bubble, complete circulation is assumed and the temperature and mass fraction fields are considered well mixed and lumped. Pressure: the vapor and liquid pressures are indential throughout collapse. Temperature: from a lumped parameter analysis, it is reasonable to assume that the inlet vapor temperature quickly rises to the vapor–liquid interface temperature.
Liquid	Flow: the velocity field can be described as a laminar axisymmetric irrotational flow altered by the radial velocity induced by bubble collapse. The temperature field, the mass fraction field, and the velocity field do not influence each other; the Dufour and Soret effects are negligible. Pressure: no variation in pressure with vertical height. Inertial effects of the liquid are negligible. Bubble absorber wall effects on the liquid are ignored.
Interface	Vapor–liquid equilibrium is assumed. Resistance: there is no interfacial resistance due to surfactants. There are no chemical reactions. Heat and mass transfer during injection are ignored. Surface tension effects only act to maintain bubble shape.

$$k\frac{\partial T}{\partial r}\bigg|_{\text{itf}} = \rho_{\text{v}} h_{\text{fg}} \dot{a}, \tag{15}$$

where the heat of condensation released at the interface is balanced by the heat removed through conduction. If we integrate (15) about the bubble surface and solve for the, $\dot{a}$

$$\dot{a} = \frac{k}{2\rho_{\text{v}} h_{\text{fg}}} \int \left[\frac{\partial T}{\partial r}(a, \theta, t)\right] \sin\theta \, d\theta \text{ at } r = a, \tag{16}$$

we can reveal how single component bubble collapse is affected by different parameters [15]. If we follow similar steps for the problem examined in this paper, the conservation of energy at the bubble interface for this problem leads to the following equation:

$$\begin{aligned} &\left[-\rho D_{\text{AB}} \frac{\partial \omega_{\text{A}}}{\partial r}\bigg|_{\text{itf}} + \rho_{\text{A}}\left(v_{\text{l, n}} - \dot{a}\right) h_{\text{A,abs}} \right] \\ &\quad + \left[-\rho D_{\text{BA}} \frac{\partial \omega_{\text{B}}}{\partial r}\bigg|_{\text{itf}} + \rho_{\text{B}}\left(v_{\text{l, n}} - \dot{a}\right) \right] h_{\text{B, fg}} \\ &\quad = -k_{\text{l}} \frac{\partial T}{\partial r}\bigg|_{\text{itf}}, \end{aligned} \tag{17}$$

where the liquid and vapor kinetic energy, the conduction into the vapor phase, and the work against viscous forces were all ignored. In Eq. (17), the heat of vaporization and dilution for each component is evaluated at the interface conditions, namely its temperature and concentration. The heat of absorption is determined from Eq. (18) [17]

$$h_{\text{abs}} = h_{\text{v}} - h_{\text{l}} - (\omega_{\text{v}} - \omega_{\text{l}}) \left(\frac{\partial h_{\text{l}}}{\partial \omega_{\text{l}}}\right)_{\text{p}} \tag{18}$$

where h_{v} and h_{l} represent the coexisting vapor and liquid states and the partial derivative represents the partial mass enthalpy. If we integrate Eq. (17) about the surface of the bubble, the rate of change of the bubble radius can be expressed as

$$\begin{aligned} \dot{a} = &\frac{1}{\dfrac{2\rho_{\text{v}}}{\rho_{\text{l}}}\left(\rho_{\text{A}} h_{\text{A, abs}} + \rho_{\text{B}} h_{\text{B, fg}}\right)} \\ &\int_0^{\pi} \left[-\rho D_{\text{AB}} \frac{\partial \omega_{\text{A}}}{\partial r}\left(h_{\text{A, abs}} - h_{\text{B, fg}}\right) \right. \\ &\left. + k_{\text{l}} \frac{\partial T_{\text{l}}}{\partial r}\bigg|_{\text{itf}} \right] \sin\theta \, \text{d}\theta. \end{aligned} \tag{19}$$

The assumption of vapor–liquid equilibrium at the bubble interface is the final boundary condition:

$$\omega_{\text{itf}} = f(T_{\text{itf}}, P). \tag{20}$$

The velocity equations (2) and (12) together with the governing conservation equations (3) and (5) with the required boundary and initial conditions equations (7)–(10), (17), and (20) form the complete mathematical problem.

Properties used in this model are taken from two sources: Jain and Gable [18] for ammonia–water mixtures and Daubert et al. [19] for pure substances.

2.3. Numerical solution

Solving this bubble absorption problem is not straightforward; it is an unsteady, two-dimensional, moving boundary/phase change problem. While a closed-form analytical solution is not known, there are numerical solution tools. The application of finite difference techniques to boundary layer partial differential equations, like (3) and (5), is well understood (Chapter 7 of [20]). When the time derivative is approximated by forward differencing or backward differencing and the spatial derivatives are approximated by central differencing, first-order accuracy in time and second-order accuracy in space is achieved. A fully implicit technique was chosen for two reasons: (1) fully implicit techniques are unconditionally stable, lacking constraints on choices of time step, Δt, or grid spacing, Δr, and $\Delta\theta$ and (2) fully implicit techniques have been proven effective for solving a wide range of transport problems.

With boundary layer finite difference approximations, where ($\frac{\partial}{\partial r} \gg \frac{\partial}{\partial \theta}$), the order of approximation in the streamwise direction can be reduced from second to first, (p. 363 of [20]). As a result, the implicit finite difference method creates a tridiagonal system of algebraic equations, allowing the implementation of the Thomas algorithm (p. 457 of [21]). The governing equations can be discretized to obtain algebraic equations of the form:

$$\begin{aligned} &\frac{\phi_{i,j}^{n+1} - \phi_{i,j}^{n}}{\Delta t} + u_{\text{r}(i,j)}^{n} \frac{\phi_{i,j+1}^{n+1} - \phi_{i,j-1}^{n+1}}{2\Delta r} \\ &\quad + \frac{u_{\theta(i,j)}^{n}}{r_j} \frac{\phi_{i,j}^{n+1} - \phi_{i-1,j}^{n+1}}{\Delta\theta} \\ &\quad = \frac{2}{\Gamma^{n} r_j^2 \Delta r} \left[r_{j+1/2}^2 \left(\frac{\phi_{i,j+1}^{n+1} - \phi_{i,j}^{n+1}}{\Delta r} \right) \right. \\ &\qquad \left. - r_{j-1/2}^2 \left(\frac{\phi_{i,j}^{n+1} - \phi_{i,j-1}^{n+1}}{\Delta r} \right) \right] + O\left(\Delta t, \Delta\theta, \Delta r^2\right). \end{aligned} \tag{21}$$

The overall accuracy of this finite difference equation is $O(\Delta t, \Delta\theta, \Delta r^2)$ [14], where ϕ equals the nondimensional concentration or nondimensional temperature.

Since the problem posed in this study involves phase change and a moving boundary condition, two ad hoc

methods are necessary to obtain a reasonable solution. First, the moving boundary can make convection dominant over diffusion in the radial direction. As a result, central differencing leads to coefficient matrices that are not diagonally dominant, which in turn leads to unstable Thomas Algorithm solutions [22,23]. To address this problem, a mesh Péclet number, Pe_{mesh}, is used to assign weighted central and upwinding differences (p. 345 of [20,24]). The mesh Péclet number is calculated with a characteristic length equal to the spacing between consecutive j values and a characteristic velocity equal to the radial velocity, which coincides with the direction of dominant diffusion. For example, the radial convection term in the conservation equations, in the case where the radial velocity, u_r, is positive, may be expressed as:

$$u_r\frac{\partial\phi}{\partial r} \cong \left(\frac{Pe^*_{\text{mesh}}}{Pe^*_{\text{mesh}}}\right)u^n_{r(i,j)}\frac{\phi^{n+1}_{i,j+1}-\phi^{n+1}_{i,j-1}}{2\Delta r} + \left(1-\frac{Pe^*_{\text{mesh}}}{Pe^*_{\text{mesh}}}\right)u^n_{r(i,j)}\frac{\phi^{n+1}_{i,j}-\phi^{n+1}_{i,j-1}}{\Delta r}, \tag{22}$$

where Pe^*_{mesh} is the critical mesh Péclet number equal to 2 (p. 344 [20]). Second, an adaptive computational grid must be employed to handle the moving liquid–vapor interface. At each new time step, the computational grid is adapted for each new bubble diameter. Once a new bubble radius is calculated at the new time step, the solution method steps in time by assigning node values based on the previous grid at the nth time level to the newly generated grid at the $n+1$ time level.

Two validation exercises were done to test the model before running it for the actual problem described here: (1) pure mass diffusion from a solid sphere ([25] pp. 69 and 70) and (2) convective–diffusive heat and mass transfer from a translating fluid sphere [26]. In each test, when comparing heat or mass transfer, this finite difference model matched the analytical solution to within $\pm 3\%$ [14].

3. Results and discussion

The following paragraphs will describe in detail, the collapse of a binary bubble enclosed within a subcooled binary liquid solution. The first series of results are based on conditions shown in Table 2. These conditions represent typical testing conditions for a bubble absorber the author has examined [16]. The absorber was made of steel tubing with a 3.6 cm inner diameter and an overall length 1.5 m. The second series of results examine the influence of the bubble size and the liquid temperature gradient on bubble collapse. While the problem described here involves heat and mass transfer occurring simultaneously, for clarity the next few paragraphs will focus on the mass transfer aspects, followed by the heat transfer aspects.

Table 2
Typical bubble absorber inlet conditions

Item	Vapor	Liquid
Bubble radius (m)	1.855e−3	–
Liquid temperature gradient (Δ°C/m)	–	62.0
Temperature (°C)	127	127
Ammonia mass fraction	0.95	0.08
Pressure (kPa)	503	503
Flow rate (g/s)	0.91	4.0

Fig. 3 uses the ammonia concentration field and the bubble wall motion to determine an average mass transfer coefficient over the bubble surface, throughout the bubble life span. Fig. 3 shows a comparison of the bubble average mass transfer coefficient calculated with the model at a particular point in time and space, and the value calculated with the following semi-empirical correlation (p. 184 of [4]):

$$\overline{Sh} = 1.13\cdot Pe_m^{1/2} \tag{23}$$

The average mass transfer coefficient for species A over the bubble interface was calculated using Eq. (24).

$$\bar{h}_m = \int_0^{\pi}\frac{-D_{AB}\left.\frac{\partial\omega_A}{\partial r}\right|_{itf}+\frac{\rho_A}{\rho}\left(u_{r,\,itf}-\dot{a}\right)}{(\omega_{itf}-\omega_{bulk})}\sin\theta\,d\theta, \tag{24}$$

where the first term in the numerator represents the diffusive mass flux inside the surrounding liquid concentration field and the second term represents convective mass flux resulting from bubble collapse.

As shown in Fig. 3, the model prediction follows the semi-empirical correlation over most of the bubble life span. Over the entire bubble life span, the average mass transfer coefficient predicted by the model and semi-empirical correlation are 1.45e−3 and 1.35e−3 m/s, respectively, a 7% difference.

Looking at Fig. 3 there can be seen several distinct stages to the absorption process. During the initial stages, the model predicts an abrupt spike in the average mass transfer coefficient. From $\approx$ 0.0–0.02 s, the interface temperature is only slightly affected by the heat removal process (Fig. 4). As the bubble continues its ascent, the surrounding decrease in bulk liquid temperature begins to impact the bubble interface temperature and concentration more significantly, increasing the mass transfer driving potential from the interface to the bulk. After passing an initial maximum at 0.05 s, the mass transfer coefficient moves towards a

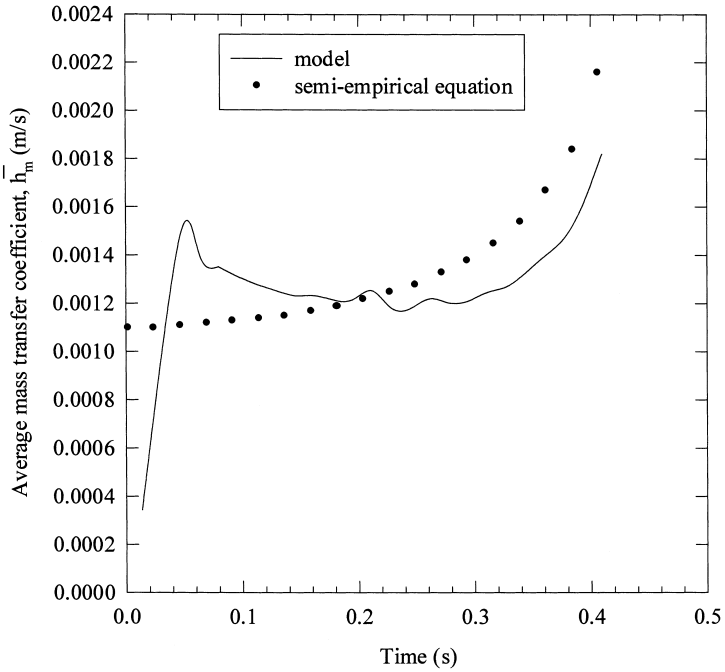

Fig. 3. Average mass transfer coefficient versus time, model prediction and semi-empirical correlation, Eq. (23).

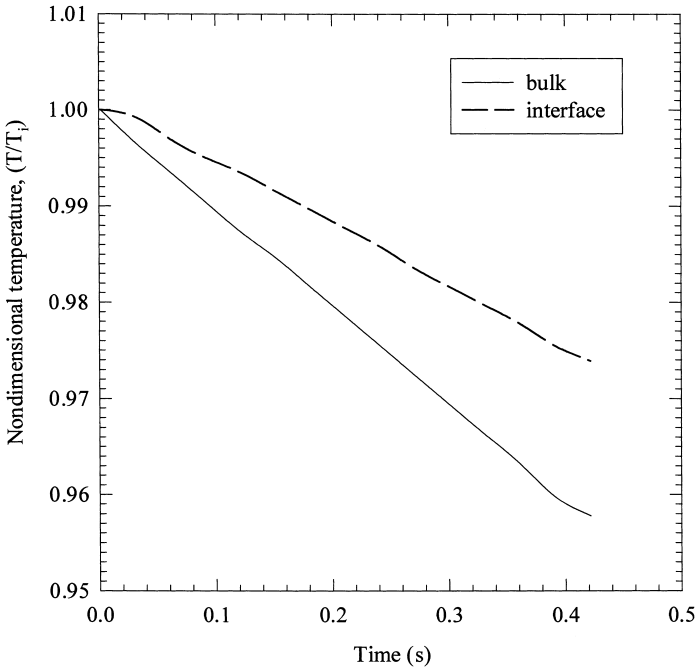

Fig. 4. Dimensionless interface and bulk temperature.

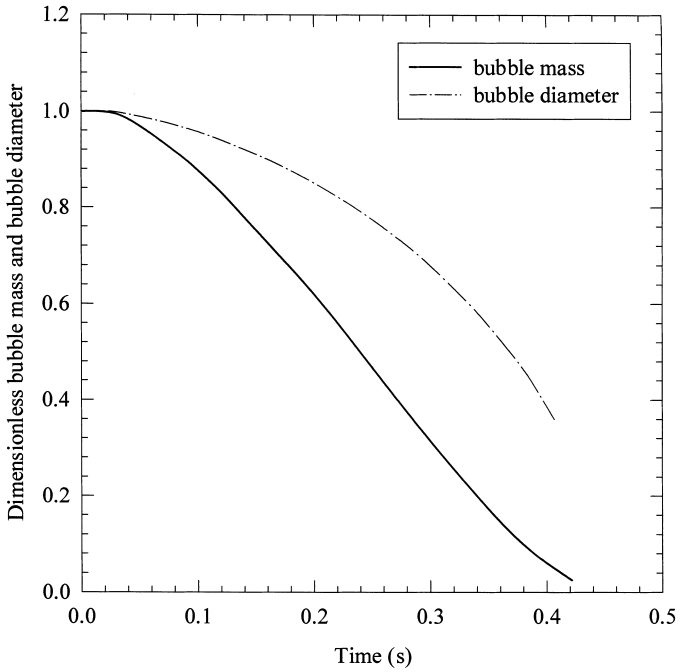

Fig. 5. Dimensionless bubble diameter and bubble mass versus bubble residence time.

local equilibrium value of nearly 1.25e−3 m/s, lasting for about 50% of the bubble life span. During this time, the rate of bubble mass removal is nearly constant (Fig. 5). In the last quarter of the bubble life span, while the bubble is slowing down, the rate of change of bubble diameter is increasing and the mass transfer coefficient reaches its second and final maximum at the time of bubble collapse, 0.42 s.

By taking a step closer and examining the behavior of each component in the binary system, the model reveals several fascinating illustrations. Fig. 6 shows, qualitatively, the directions of mass transfer during collapse resulting from diffusion and convection. Using the model, if we sum the values of each flux vector of each component, the net effect is mass removal of ammonia and water from the bubble (Fig. 7). Fig. 8 shows the convective and the diffusive mass transfer for ammonia (Eq. (13)). It also illustrates some instability with the numerical method chosen here. Fig. 9 shows the convective and diffusive mass transfer for water (Eq. (14)). To remove water, the absorbate, from the bubble core, water counter-diffusion is off-set by the water convection resulting from the bubble interface collapse.

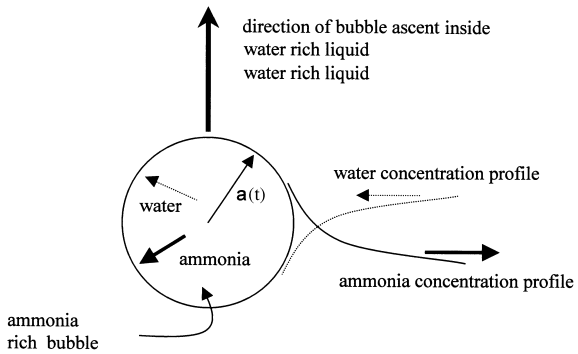

Fig. 6. Mass transfer flux vectors for each component during bubble life span.

As each molecule of ammonia or water travels from the vapor core to the bubble interface, energy is released as these molecules are condensed and mixed in the surrounding liquid solution. A net release of energy acts to increase the interface temperature and reduce the interface concentration, extending the bubble life span. Unfortunately for the bubble, the liquid surrounding it cools the bubble wall, increasing the interface concentration and accelerating the demise of the bubble. In an attempt to predict this dynamic heat transfer process, Eq. (23) was modified for a heat transfer process; the Pe_m is replaced with the heat transfer Peclet number, Pe:

$$\overline{Nu} = 1.13 \cdot Pe^{1/2}. \tag{25}$$

Fig. 10 shows a comparison of the bubble average heat transfer coefficient along the bubble ascent calculated

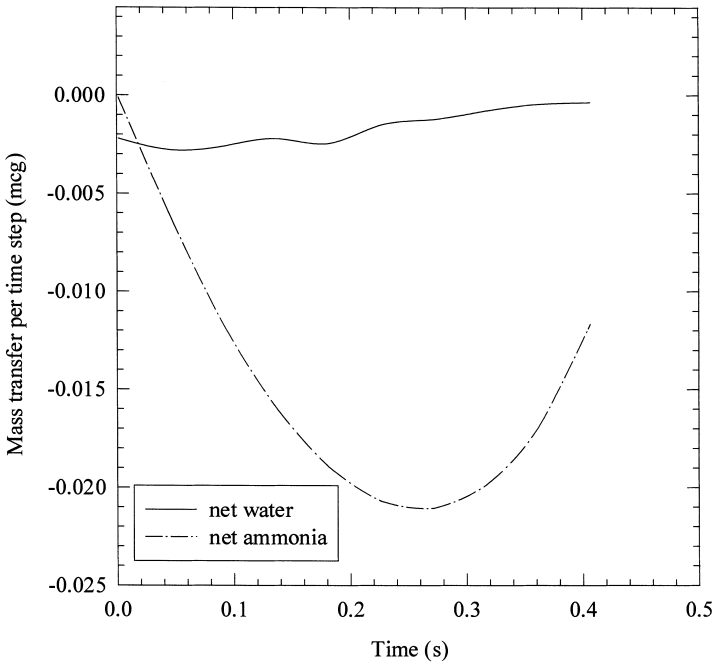

Fig. 7. Net ammonia and water mass transfer per time step over the bubble life span (time step is 0.1 ms).

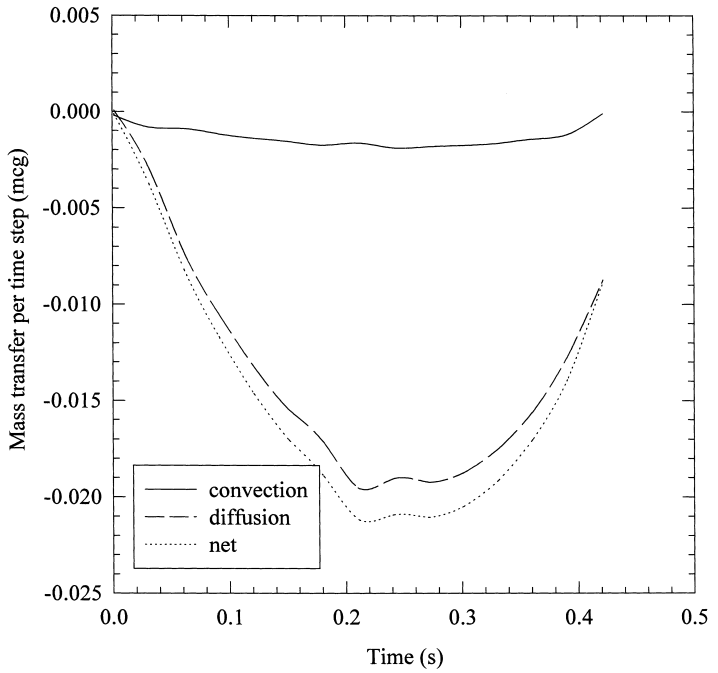

Fig. 8. Ammonia mass transfer per time step over the bubble life span (time step is 0.1 ms).

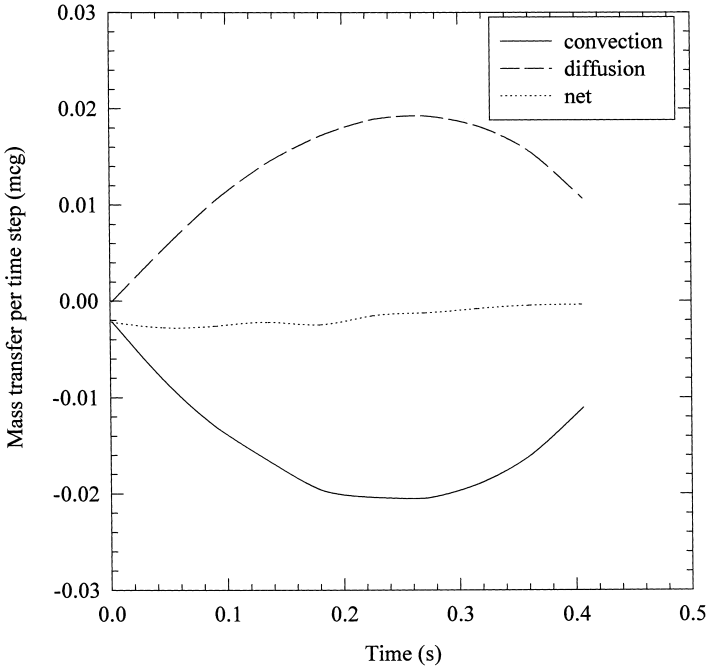

Fig. 9. Water mass transfer per time step over the bubble life span (time step is 0.1 ms).

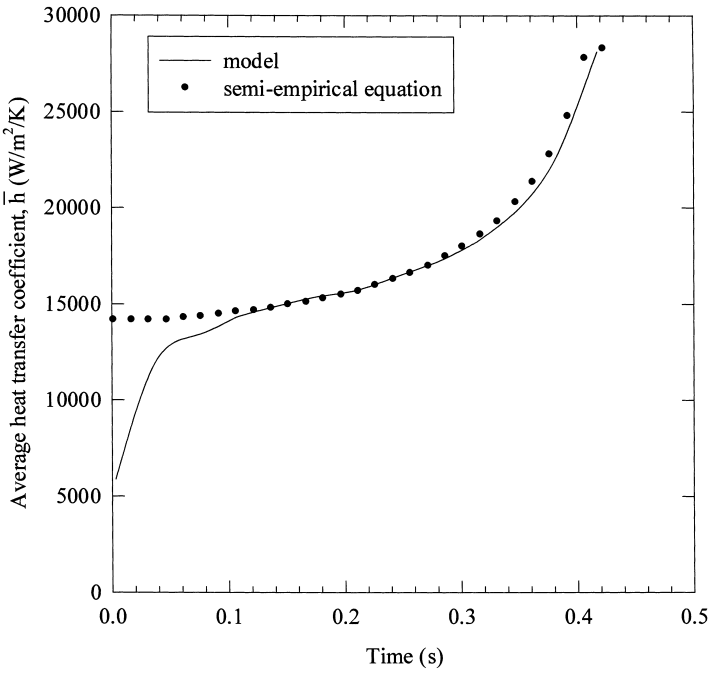

Fig. 10. Average heat transfer coefficient versus time, model prediction compared and semi-empirical correlation, Eq. (25).

with the model and the value calculated with Eq. (25). The average heat transfer coefficient found with the model was calculated using Eq. (26). The first term in the numerator represents diffusion of heat from the bubble interface into the surrounding subcooled liquid and the second term represents convection of heat for each species due to the bubble collapse.

$$\bar{h} = \int_0^{\pi} \frac{-k_1 \left.\frac{\partial T}{\partial r}\right|_{\text{itf}} + \sum_i^I \rho_i \left(u_{\text{r, itf}} - \dot{a}\right) h_{\text{f, }i}(T_{\text{itf}})}{(T_{\text{itf}} - T_{\text{bulk}})} \sin\theta \, \mathrm{d}\theta \tag{26}$$

The average heat transfer coefficient over the bubble life span predicted by the model is 16,700 W/m^2/K compared with 17,500 W/m^2/K from Eq. (25), only a 4.5% difference.

Having shown that the model provides reasonable predictions to binary bubble collapse behavior, let us examine two parameters that can be changed within typical bubble absorbers: the inlet injection port size and the rate a which the subcooled liquid is cooled (Fig. 1).

Fig. 11 shows that the approximate bubble collapse time (time required to reach 10% of the original bubble mass) changes linearly with initial bubble radius. All the other parameters shown in Table 2 are assumed held constant. In the range of conditions modeled here, Fig. 11 shows that the rate of mass absorption increases with the square of the radius, since the volume or mass increases with the cube of radius and the time of collapse increases linearly with radius. However, while larger bubbles do, in general, rise more quickly, increasing the mass transfer Peclet number, coalescence among many bubbles may reduce absorption rates by eliminating the effective mass transfer surface area.

The rate of heat removal from the surrounding subcooled liquid can also be altered. Fig. 12 shows the effect of changing the subcooled liquid temperature gradient along the z-direction, the direction along the bubble ascent (Fig. 2). Cooling the liquid more rapidly surrounding a collapsing bubble decreases the collapse time. Fig. 12 also shows that after a liquid temperature gradient of about 90 C/m, the rate of collapse begins to plateau. Picking the optimum cooling rate would require a global look at the entire absorption cycle. In an actual absorber, if heat is removed too rapidly, significant subcooling can occur, seriously reducing the overall cycle efficiency.

4. Conclusion

The behavior of single bubble collapse with substantial thermal effects has been modeled. Beginning with species conservation, energy conservation, and several boundary conditions based on actual bubble absorption testing, the mathematical problem of bubble collapse was solved using a finite difference approach.

The model appears to predict bubble collapse accurately. Looking at the overall bubble heat and mass transfer during collapse, the model matched simple semi-empirical equations closely. Further experimental measurements with actual binary bubbles in subcooled liquid solutions are needed to confirm if both approaches are accurate.

It was also shown that the counter-diffusion of the absorbate towards the bubble, which acts to preserve bubble size, is off-set completely by convective mass transfer arising from bubble interface motion.

By examining two bubble absorber design issues it was shown that bubble collapse rates increase proportional to the radius squared (for bubbles diameters 1.8–5.6 mm). Increase in the subcooled liquid tempera-

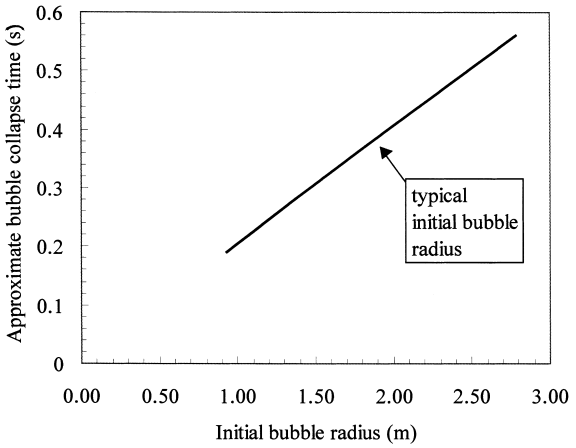

Fig. 11. Approximate bubble collapse time versus bubble radius.

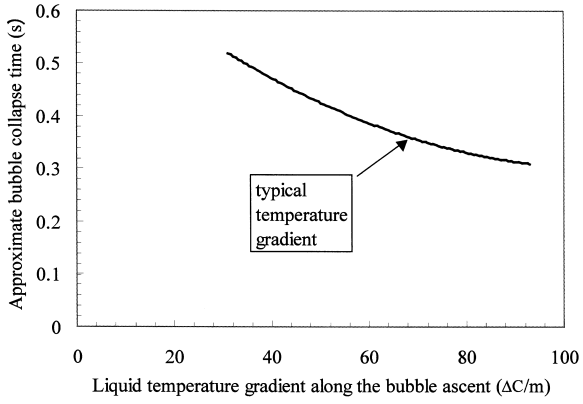

Fig. 12. Approximate bubble collapse time versus liquid temperature gradient along bubble ascent.

ture gradient increased bubble collapse rates, to a point. At an ≈ 90 C/m temperature gradient along the length of the bubble's ascent, improvements in bubble collapse rates plateau.

While this paper has attempted to give insight into the inner dynamics of bubble absorption in binary solutions, there are two important elements this model does not take into account: the effect of bubble swarms, and the impact of bubble absorber design changes on overall absorption cycle performance. To effectively design bubble absorbers for absorption chillers, future work should focus in three areas: (1) single bubble basic experiments to confirm and improve model predictive capabilities, (2) model development and experimental confirmation of bubble swarms, and (3) the integration of an accurate bubble swarm model with an equally accurate absorption cycle model.

Acknowledgements

The author gratefully acknowledges the encouragement and support of Dr. Horacio Perez-Blanco at The Pennsylvania State University, and Mr. Tetsuo Setoguchi at the Osaka Gas Company. In addition, private communication with Professor Gershon Grossman and Professor Keith Herold were very helpful.

References

[1] V.G. Levich, Motion of gaseous bubbles with high Reynolds number, Zhn. Eksp. Teor. Fiz 19 (1949) 18–24.
[2] B.T. Chao, Motion of spherical gas bubbles in a viscous fluid at large Reynolds numbers, J. Fluid Mechanics 25 (1962) 69–79.
[3] D.W. Moore, The boundary layer on a spherical gas bubble, J. Fluid Mechanics 16 (1963) 161–176.
[4] D. Azbel, Two-Phase Flows in Chemical Engineering, Chapters 1, 2, 3, and 7, Cambridge University Press, New York, NY, 1991.
[5] L.W. Florschuetz, B.T. Chao, On the mechanics of vapor bubble collapse, J. Heat Transfer 87 (1965) 209–220.
[6] T. Elperin, A. Fominykh, Cell model nonisothermal gas absorption in gas–liquid bubbly media, Heat and Mass Transfer 31 (5) (1996) 307–311.
[7] G. Grossman, Simultaneous heat and mass transfer in film absorption under laminar flow, Int. J. Heat Mass Transfer 26 (3) (1983) 357–371.
[8] G.C. Vliet, J.W. Andberg, A simplified model for absorption of vapors into liquid films flowing over cooled horizontal tubes, ASHRAE Transactions 93 (2) (1987) 1–15.
[9] J.S. Seewald, H. Perez-Blanco, A simple model for calculating the performance of a lithium-bromide/water coil absorber, ASHRAE Transactions 100 (2) (1994) 318–328.
[10] V. Patnaik, H. Perez-Blanco, An empirical methodology for the design of vertical tube absorbers, ASHRAE Transactions 102 (2) (1996) 185–196.
[11] N.I. Grigor'eva, V.E. Nakoryakov, Exact solution of combined heat and mass transfer problem during absorption, Inzhenerno-Fizicheskii Zhurnal 33 (5) (1977) 893–896.
[12] C. Ruh, J.M. Smith, Theoretical investigation of gas side mass transfer resistance in a hot stirred tank reactor, in: Proceedings of the 1996 Fluid Mixing 5 Conference, Bradford, U.K., vol. 140, 1996, pp. 339–345.
[13] T.L. Merrill, H. Perez-Blanco, Combined heat and mass transfer during bubble absorption in binary solutions, Int. J. Heat Mass Transfer 40 (3) (1997) 589–603.
[14] T.L. Merrill, Bubble heat and mass transfer dynamics in binary solutions, Mechanical Engineering Ph.D. Thesis, The Pennsylvania State University, University Park, PA, 1994.
[15] D.D. Wittke, Collapse of vapor bubbles with translatory motion — a theoretical and experimental investigation, Ph.D. Thesis, University of Illinois, Champaign-Urbana, IL, 1966.
[16] T.L. Merrill, T. Setoguchi, H. Perez-Blanco, Passive heat transfer enhancement techniques applied to compact bubble absorber design, Journal of Enhanced Heat Transfer 2 (3) (1995) 199–208.
[17] F. Bosnjakovic, Technical Thermodynamics, Holt (P.L. Blackshear, Trans.), Rinehart and Winston, 1965.
[18] P.C. Jain, G.K. Gable, in: Equilibrium property data equations for aqua-ammonia mixtures, ASHRAE Semiannual Meeting, Philadelphia, PA, January, 1971.
[19] T.E. Daubert, R.P. Danner, H.M. Sibul, C.C. Stebbins, Physical and Thermodynamic Properties of Pure Chemicals: Data Compilation, Taylor and Francis, Bristol, PA, The Pennsylvania State University Chemical Engineering Dept, 1997.
[20] D.A. Anderson, J.C. Tannehill, R.H. Pletcher, Computational Fluid Mechanics and Heat Transfer, Hemisphere, New York, NY, 1994 (Chapters 1–12).
[21] C. Hirsch, Numerical Computation of Internal and External Flows, vol. 1, Wiley, New York, NY, 1988 (Chapters 1–12).
[22] S.V. Patankar, D.B. Spalding, Heat and Mass Transfer in Boundary Layers, Morgan-Grampian Books, London, 1967 (Chapters 1–5).
[23] R.S. Hirsh, D.H. Rudy, The role of diagonal dominance and cell Reynolds number in implicit methods for fluid mechanics problems, J. Comp. Phys 16 (1974) 304–310.
[24] D.B. Spalding, GENMIX: A General Computer Program for Two-dimensional Parabolic Phenomena, Pergamon Press, New York, NY, 1997 (Chapters 1–11).
[25] T.K. Sherwood, R.L. Pigford, C.R. Wilke, Mass Transfer, McGraw-Hill, New York., NY, 1975.
[26] B.T. Chao, Transient heat and mass transfer to a translating droplet, J. Heat Transfer 91 (1969) 273–281.